Multiphysics FEA Modelling of Gasketed Bolted Flange Joints

Jan Oredsson

Pipeotech AS; Molandsveien 10, 4994 Akland, Norway

Juan Manuel Paz García (supervisor)

University of Malaga (UMA), Malaga, Spain

Abstract. Gaskets play an important role in the sealing performance of bolted flange joints and especially in its key task to reduce fugitive emissions which can be detrimental to the environment. Their behaviour is complex due to nonlinear material properties combined with permanent deformation. Industry experience shows that the achievement of a leak proof joint depends on many parameters such as gasket/flange contact stress and flange rotation. Several fields of physics are involved in the leakage performance of a bolted flange joint, namely mechanical displacement, fluid flow and electrolyte potentials.

In this Master Thesis paper, several finite element analysis models (2D axisymmetric and 3D) have been developed and tested applying the COMSOL Multiphysics software considering DeltaV-Seal, a fully metallic gasket. The model results have been compared with the results of standard gasket laboratory testing and time to failure of the gasket due to galvanic corrosion have been simulated in a 1-year simulation. The paper also addresses the demanding task to adequately model the structural contact between the knife-edge sharp DeltaV-Seal ridges and the flange surface during bolt-up of the flange joint.

The work presented in this Master Thesis paper is Phase 1 of an ongoing R&D project partly funded by the Research Council of Norway (SkatteFUNN). In subsequent phases of the project the different sub-models will be integrated into a multi-physics knowledge platform which will be made accessible via dedicated applications distributed to relevant stakeholders.

1. INTRODUCTION

Gasketed piping and vessel flange joints leak and cause fugitive and other types of emissions which may be harmful to the environment.

PoT is a global designer, manufacturer, and supplier of fully metallic gaskets with a current product library consisting of over 200 products of different materials and dimensions. There is an ongoing R&D project to increase product development and supply efficiency by developing an IT-based knowledge platform and associated Applications that can be utilized by PoT's stakeholders (engineers, sales personnel, and customers). The project is partly funded by the Research Council of Norway.

FIG. 1. Process plant with pointwise emissions

PoT's fully metallic gasket product is called DVS and provides sealing by several sharp rings or ridges acting as the barrier to leakage systematically distributed on a core. These rings are compressed during the bolt pre-tension providing a tight seal, typically to 4-15% thickness compression.

Measured leak rates across the leak path between the compressed sealing rings and the interfacing flange surfaces are in the range of 10^{-7} to 10^{-6} mg/m/s (mass flow) depending on the conditions.

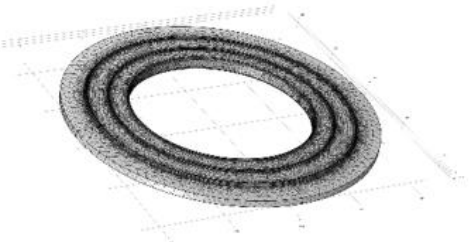

FIG. 2. DN40 DeltaV-Seal modelled with shape optimization

A gasketed BFJ is a complex system of movable parts (flange, bolts, nuts, washers, and gasket). This system can be considered as a system of axial/parallel springs with different spring constants with at least two contact areas, namely the DVS/flange (Case A) interface and the flange ring/bolt head interface (Case B). These system properties make numerical modelling quite challenging and especially so for Case A due to the knife-edge type of contact that must be considered in the modelling.

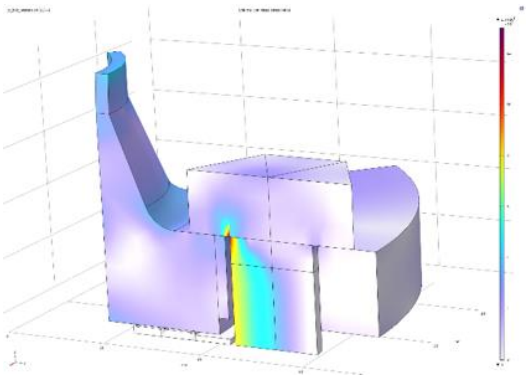

FIG. 3. Part of bolted flange joint with loads

Several FEA-based investigations/publications exist on the mechanical behaviour of BFJ but none of these considers the integration of other fields of physics impacting on the leakage performance of BFJ (5).

Leakage of gasketed BFJ involves several different physical fields such as mechanical displacement fields, fluid flow fields and electrolyte potential fields. The uniqueness of this modelling lies in integration of these fields into a single model that simulates the leakage for varying flange joint dimensions and types of fluids by applying a suitable multi-physics integrating software platform like COMSOL Multiphysics.

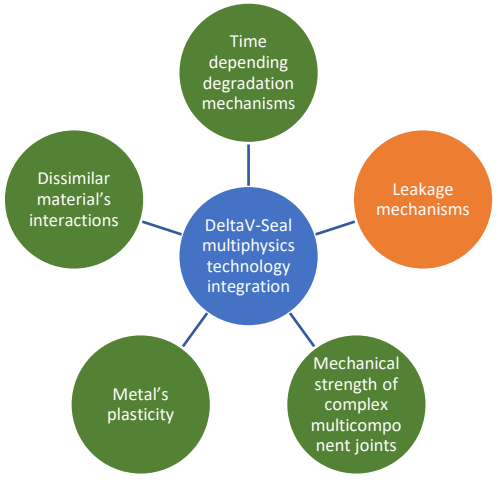

FIG. 4. Integration of fields of physics in knowledge platform

PoT has performed several laboratory testing programs of DVS. These programs have provided test data that have been implemented in the project and that will serve as validation of the developed model performance.

The objective of this Master Thesis is to develop new and/or fine-tune PoT's existing sub-models for the different applicable fields of physics. Eventually these sub-models will be integrated in one simulation model in future R&D projects, see below.

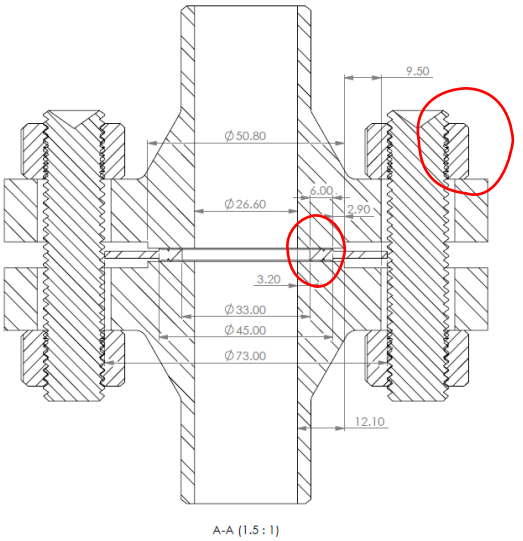

FIG. 5. Internal and external galvanic corrosion cells in bolted flange joints with metallic gaskets

The electrolyte potential fields created inside BFJ may cause degradation of the gasket due to galvanic corrosion if not properly managed by material selection and may be a serious threat to the integrity of the BFJ. Internal galvanic corrosion between gasket and flange (considered in the models). There are two areas circled in the figure where galvanic corrosion may occur:

- Internal galvanic corrosion between gasket and flange (considered in the models)
- External galvanic corrosion between bolt/nut/washer and the flange rings (not considered in the models)

The metal plasticity physics of DVS is especially challenging due to the extremely small material volume contributing to the tightness of the BFJ. A standard DVS DN40 product contains in total approximately 35 mm3 of material heavily plasticised which must be properly modelled and simulated to demonstrate leak tightness of the BFJ. The flow fields of physics applicable to the leakage simulations will be modelled based on (7) during the next phases of the project.

2. MATERIALS AND METHODS

2.1. Experimental work

The main types of laboratory testing programs and obtained test results are:

- Electrochemical polarisation curves of DVS cut-outs providing applied current – electrochemical potential functions for the secondary/tertiary current distributions (Type 1).

- Mechanical compression of round bars providing stress-strain curves for the DVS material modelling functions (Type 2).
- Standardized mechanical compression of full DVS samples between flat and solid platens (EN 13555) providing applied force – DVS thickness and leakage functions for validation of the simulation models (Type 3).
- Complete BFJ gasketed with DVS tested and leakage rates determined as function of applied bolt pre-tension, pressure medium, temperature, pressures, etc. for validation of the simulation models (Type 4).

2.2. Electrochemical polarization curves (Type 1)

An extensive testing program has been performed at QEERI where DVS cut-outs were prepared and polarized in 0.5 M NaCl at ambient temperature in a standard three-electrode polarization cell.

FIG. 6. A connecting cable insulated in red to the DVS sample, moulded in Bakelite and the capillary tip of the reference electrode (SCE) applied in the glass cells.

The figure below shows a typical example of the current density response to polarization of a DVS sample compared with a sample made of a standard flange material. Decisive for the risk of galvanic corrosion is the position of the corrosion potential of the two components with respect to each other. The shown case is the preferred one since the gasket is cathodic to the flange surface and would be galvanically protected by the flange which (in theory) would be subjected to some galvanic attack close to the connection points with the DVS. However, due to the large anode/cathode area ratio, the local corrosion rate of the flange will be less critical. Furthermore, referring to the rule-of-thumb in the corrosion industry of a maximum recommended corrosion potential difference of 200 mV, the case shown in Figure 7 would be an acceptable flange/gasket (DVS) configuration.

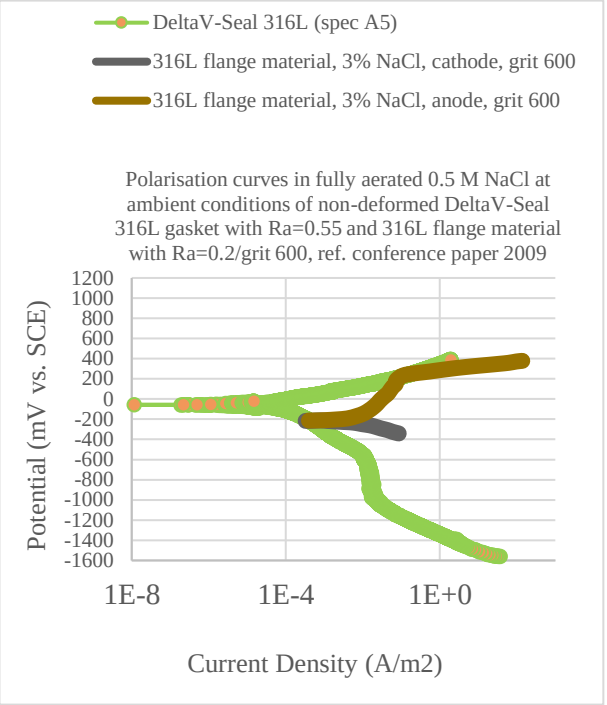

FIG. 7. Polarisation curves in fully aerated 0.5 M NaCl at ambient conditions of non-deformed DeltaV-Seal 316L gasket with Ra=0.55 and 316L flange material with Ra=0.2/grit 600, ref. conference paper 2009

2.3. Mechanical compression of round bars (Type 2)

The objective of this testing was:

- Determination of the compression yield stress (Rp0.2) of the 800HT gasket material at ambient and elevated temperature.
- Determination of the compression ultimate stress (Rc) of the 800HT gasket material at ambient and elevated temperature.
- Determination of the engineering stress-strain as well as true stress-strain relationship of the 800HT gasket material at ambient and elevated temperature.

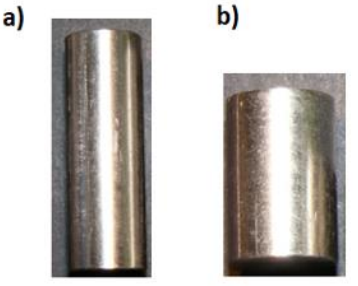

FIG. 8. a) samples shape for determination yield stress Rp0.2 with diameter 12 mm and height 36 mm (h=3xD). b) samples shape for determination ultimate compression stress were diameter 10 mm and height 15 mm (h=1.5D)

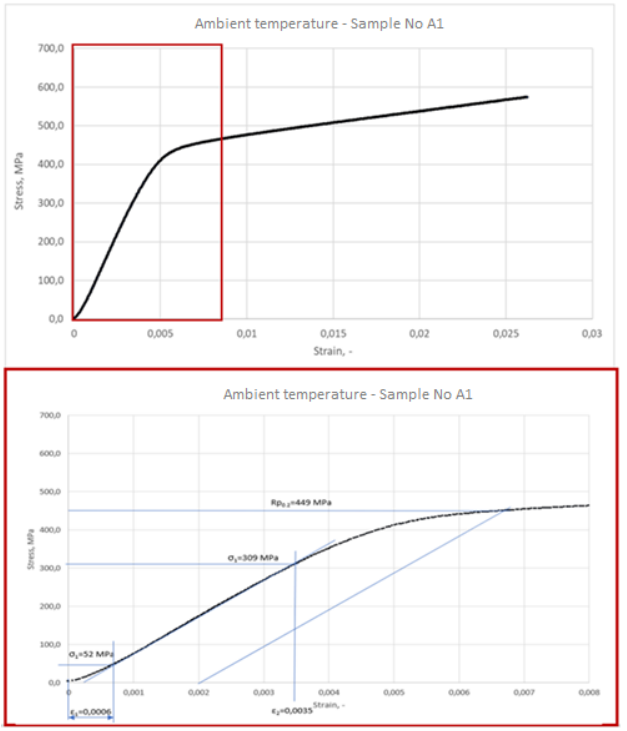

FIG. 9. Typical stress-strain curves obtained for evaluation of the yield properties are shown here.

The barrelling effect during compression and the sample diameter as a function of strain level is shown here. The true stress-strain function implemented in the models considers the significant barrelling which would otherwise invalidate the data due to unknown stress state at the boundaries of the barrelled samples.

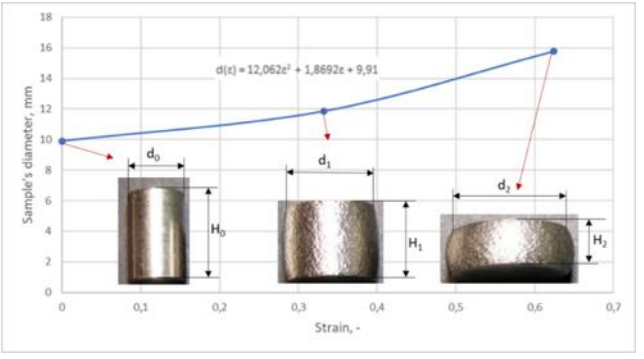

FIG. 10. Test cylinder barreling during compression testing (sample diameter as a function of strain level)

Typical stress-strain curves obtained in the compression testing are shown here. The stress-strain curve for test sample B1 has been implemented as the hardening function (interpolation function) in the DVS plasticity node in the solid mechanics physics interfaces applied in the models.

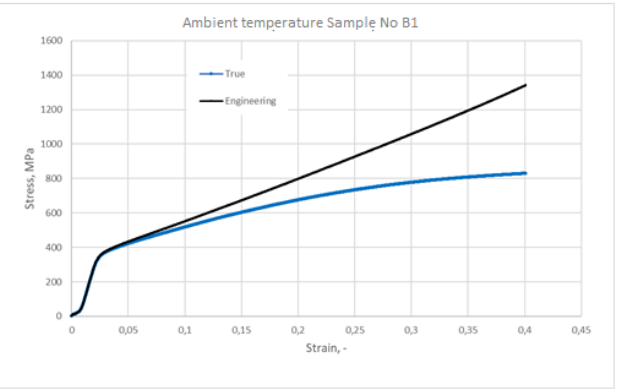

FIG. 11. Typical stress-strain curves obtained during compression testing (black: engineering; blue: true)

2.4. Mechanical compression testing to EN 13555 (Type 3)

The test sample (DVS) was placed on the lower (fixed) platen of the hydraulic press and the upper (movable) platen compressed the sample at the compression load. The two platens were equipped with transducers to measure the actual gasket thickness. Additional equipment of the test rig (among others) are: helium leakage spectrometer, pressure gauges enabling measurement of the leakage by differential pressure, the unit for platens temperature control, computer for registration, and collection of measured data. This testing is performed fully in accordance with the international gasket testing standard EN 13555.

Figure 12 below (upper graph) shows a typical gasket thickness – applied force test result. In this case, the alloy 800HT curve (brown) has been used for tentative validation of the 2D axisymmetric model, see below. In addition to the mechanical response of the gasket, the EN 13555 testing program includes determination of the leakage properties of the gasket under internal pressure, normally consisting of 40 bar helium.

Also in Figure 12 below (lower graph), the figure shows a typical leak rate – applied gasket stress plot under 40 bar internal pressure with loading curve in blue and the unloading curves shown in colours. These curves will be used as the initial benchmark for the next stage of the simulation model development where the mathematical leakage model will be codified and implemented in the full model.

In the final stage of the project, the full BFJ model leakage performance will be benchmarked against Type 4 laboratory testing, see below.

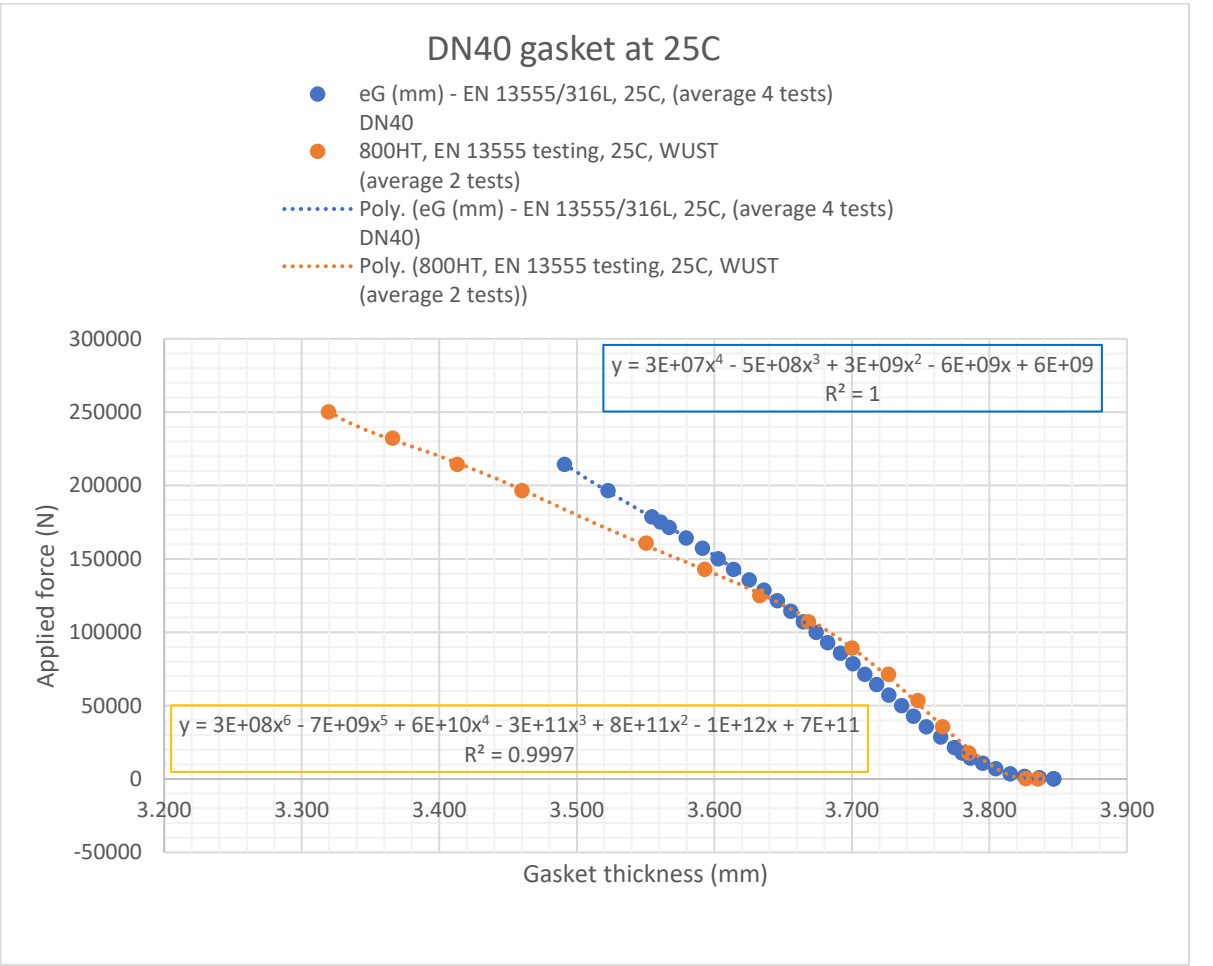

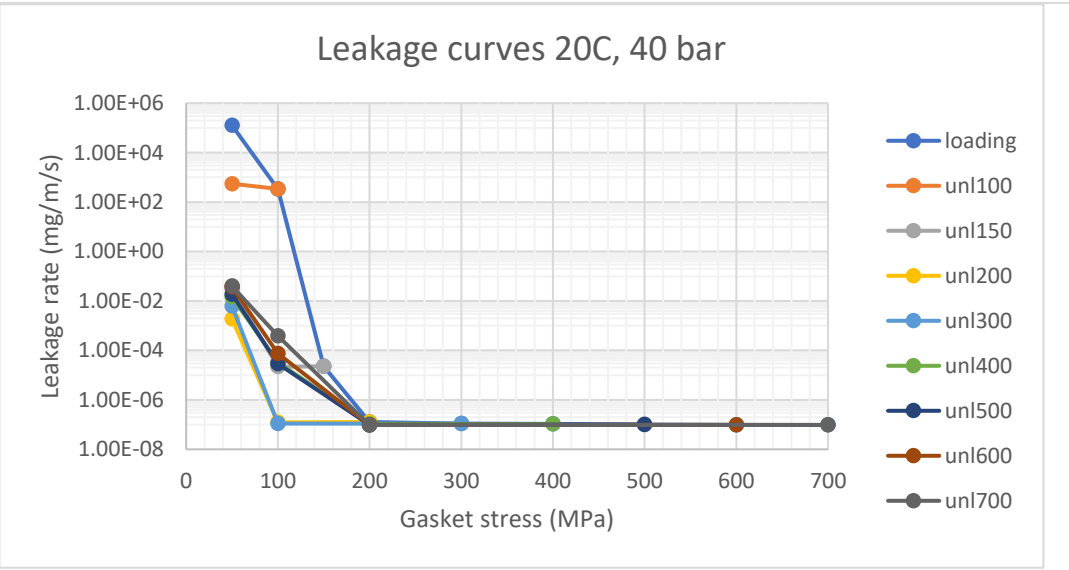

FIG. 12. EN 13555 testing (compression curves, upper graph; leakage curves, lower graph)

2.5. BFJ with DVS testing (Type 4)

PoT has also performed full-scale leakage testing of bolted flange joints gasketed with DeltaV-Seal, in this case at cryogenic conditions (liquid nitrogen at -196°C). The test set-up is shown in Figure 13. below.

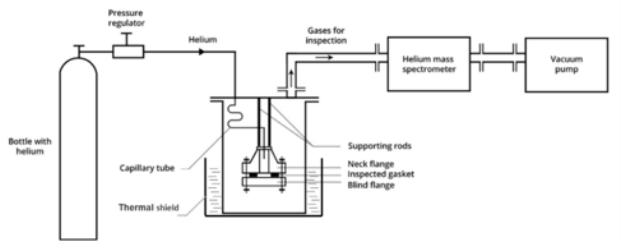

FIG. 13. Schematic of test rig for full-scale leak rate testing of bolted flange joint gasketed with DVS. PoT has performed such testing at cryogenic conditions (-196C).

The obtained results are shown in Figure 14 below.

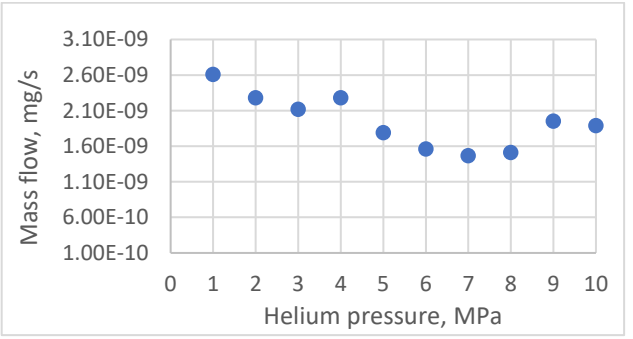

FIG. 14. Mass flow leakage as a function of internal helium pressure

Typical leak rate (mass flow) – applied pressure function for a DN40 PN40 BFJ gasketed with DVS and bolted up with a total clamping force of roughly 250 kN spread over the 4 bolts, meaning 62.5 kN per bolt.

These data will be used for validation of the integrated model.

3. MODEL DEVELOPMENT

3.1. Status/Summary

As stated in Section 1, the strategy has been to develop sub-models and then to integrate these sub-models into a full and final model which will form the basis for development of Applications. The planned sub-models with their current development status are as follows:

- Corrosion model: a 2D axisymmetric draft COMSOL model is available for simulation of time to leak due to galvanic corrosion.
- Mechanical model (1): a 2D axisymmetric draft COMSOL model is available for simulation of the DVS compression response under solid platens.
- Mechanical model (2): a 3D draft COMSOL model is available for simulation of a BFJ gasketed with DVS after bolt pre-tension and subsequent service loads (internal inert gas pressure and external piping loads).
- Leakage model: a mathematical leakage model has been developed for metal-to-metal contact surfaces representing the interface sealing surface between the gasket and flange surface. The first part of this work has provided the basic information about how to model the roughness profile using fractal theory. The second part was focused on modeling the radial flow through the porous structure in the form of cylinder proposed by Darcy. The Darcy model connected with the fractal roughness model has been successfully used to predict the leakage through the intermediate micro porous surface, that occurs at the gasket-flange contact. This model has not yet been codified into a COMSOL model.
- The final stage of this development project will be integration of the sub-models into one single model and verification using experimental testing.

3.2. The gasket

As mentioned above, the key component of a bolted flange joint is the gasket which provides the sealing ability of the joint supplying the key performance factor of the joint in terms of leak rate.

Figure 15 shows the model of 1/8 part of a full DVS DN40 product with (in this case) three sealing rings distributed across the gasket core. The standard thickness of DVS is 3.8 mm across the ridges from one side to the other. In the as-machined condition the knife-edge sharp ridges consist of 60 degrees top angled triangles with a standard height of 0.5 mm (current DVS design).

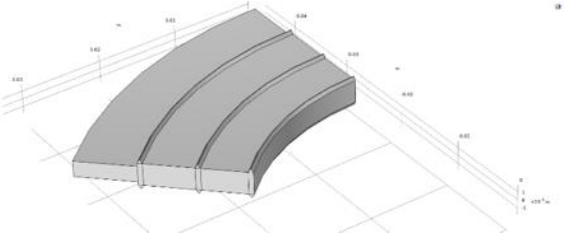

FIG. 15. Model of 1/8 part of a DVS DN40 product

After standard DVS design compression normally to a thickness reduction of 4-15%, the width in radial direction of the flattened contact areas is approximately 50-150 microns depending on the local conditions (flange surface finish, materials, etc.), refer to macro photo to the left. The rounded boundaries are due to the tooling tip with radius 0.4 mm normally applied during the turning manufacturing of these products.

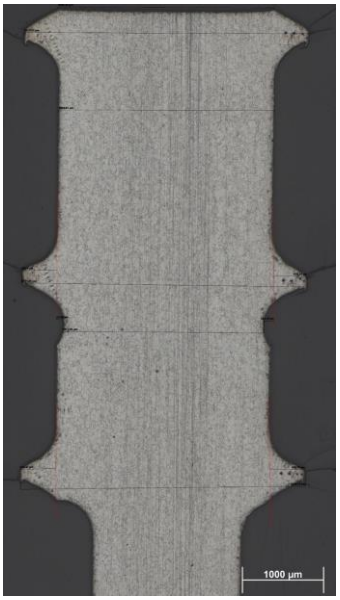

FIG. 16. Macro photo of cross section of a compressed DVS DN40 (etched in V2A)

3.3. Geometric and material properties

The modelled flange joint is a standard EN 1092-1 WN RF flange in pressure class PN40 and size DN40 with standard M16X2 bolting (3D mechanical modelling). The modelled gasket is a standard PoT DVS DN40 product.

The flange and the bolt material properties are assumed to be homogeneous, isotropic, and linearly elastic based on Young's modulus and Poisson's ratio. Materials selected for the bolt and the flange are normally the same material as the gasket to avoid dissimilar material issues like differential thermal expansion and galvanic corrosion which may cause leakage of the BFJ. The flange and the bolt material have been modelled with typical elastic properties of the UNS N08811 Fe-Cr-Ni alloy (3D modelling). Thus, the DVS material is also modelled in UNS N08811 Fe-Cr-Ni alloy but in this case with a non-linear hardening function based on laboratory compression testing of round bars, refer to Section 2.4.

3.4. Modelling features

3.4.1. Mechanical models

At the outset of the modelling work, it became clear that the choice of chamfer versus fillet versus having a sharp edge on top of the ridge was going to have a large impact on the outcome of the modelling including the penetration into the flange domain and thereby the convergence. It also became clear that this decision needed to be made on the background of selected simulation process. Furthermore, modelling of the BFJ/DVS combination with several nonlinear processes involved (contact and plasticity in this case) had to be managed in an efficient way.

The first process (contact) turned out to be the most challenging part of the project where the task was to find an acceptable model of the contact problem between the initial knife-edge geometry of the as-machined DVS interfacing with the flange surface. This interfacing transforms the ridge tops into a flattened configuration providing the tight sealing after the bolt pre-tension step. The selection of the final forming type in the Geometry sequence (Assembly or Union) turned out to have a large impact on the modelling/simulation results.

The performance of the contact modelling has been bench-marked against the numerous experimental studies of the impact on flange surfaces that PoT has conducted, refer to Figure 17 and 18 below.

FIG. 17. Raised face part of flange surface with machined concentric serrations and 3-ridge DVS interactions

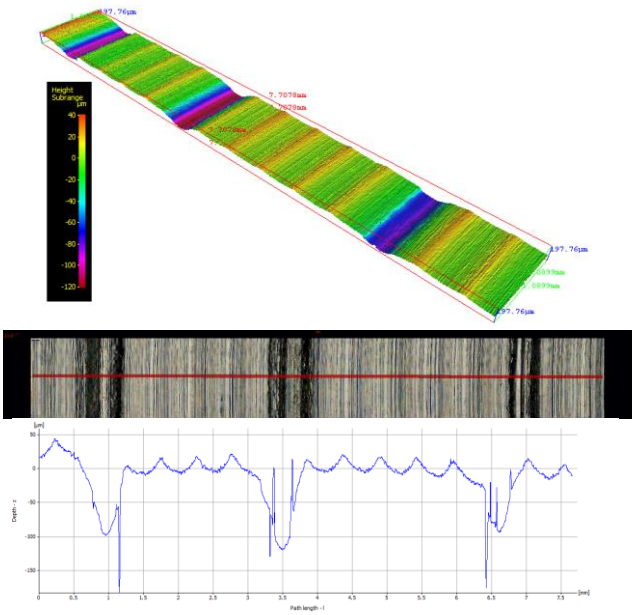

FIG. 18. The results of fractal investigations show that the ring impressions have a depth of 30-150 microns depending on numerous parameters like installation torque and materials

For solving this problem, the contact pairing method has been applied and the contact surface boundary included both the sides and the top chamfer/fillet radius of the 60 degrees ridge top triangle depending on the selected space dimension (2D axisymmetric or 3D).

The penalty contact method was selected and the penalty factor tweaked by adjustment of the penalty factor multiplier. Furthermore, in the 3D models, a friction and a stabilization node were added separately to both the gasket/flange and the bolt head/flange contacts thereby allowing application of different friction and stabilization properties to the two contacts. By this method, acceptable penetration into the flange modelling domain has been obtained in addition to healthy computation/convergence times.

It was also observed in some cases that the mesh got damaged during early stages of compression and hence a solution was needed to reach convergence, see Figure 19 lower plot for mesh damage on the DVS single domain case.

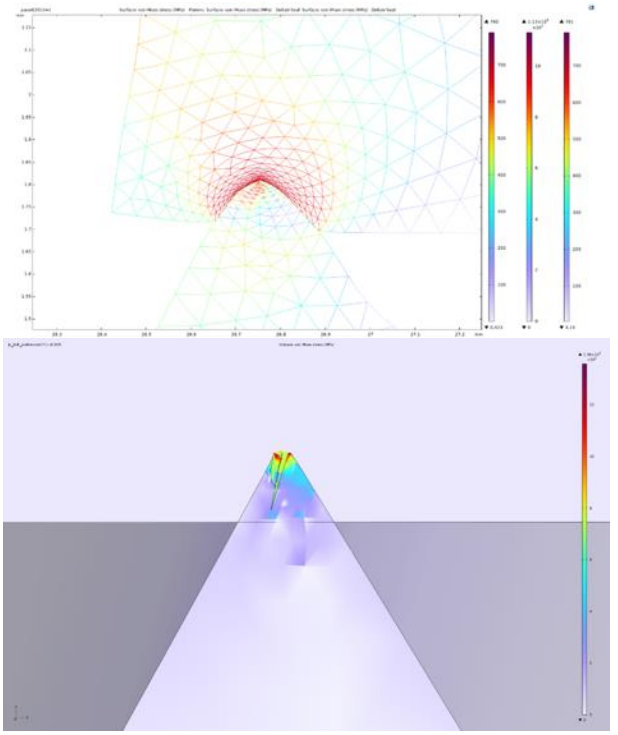

FIG.19. The upper plot shows an example of the obtained penetration in one of the 2D axisymmetric models from the early-stage modelling (in this case penetration but no mesh damage).

After extensive tweaking of the model parameters an acceptable flattening performance has been achieved for the 2D axisymmetric modelling whereas it has been more difficult to achieve the same for the 3D modelling, see Figure 20 below showing the deformed mesh after flattening of the ridge top and nicely replicating the physical behaviour seen in the laboratory, refer to the macro photo in Figure 16.

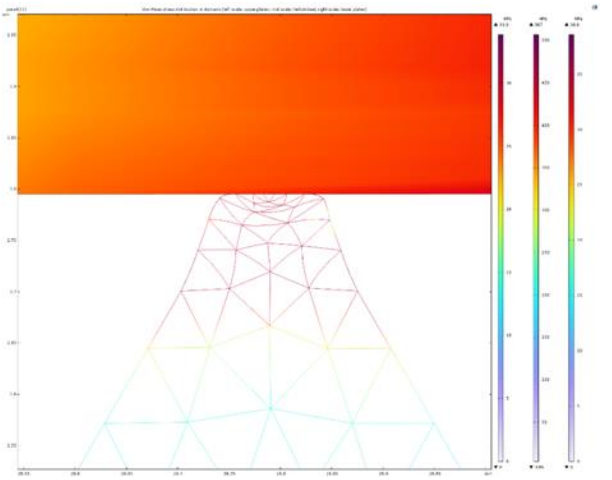

FIG.20. Mesh deformation during 2D axisymmetric modelling

The exact reason for this is not clear and needs further investigation. However, it is likely that the fundamental differences between a displacement-controlled loading with an even load line and a bolt force-controlled lever arm configuration has an impact on this issue

An extensive contact parameter investigation has been performed on the 3D model to find a solution to the poor convergence performance where the following contact parameters have been systematically varied:

- Number/type of contact boundaries.
- Touch/no-touch of contact surfaces (flange/DVS).
- Contact method.
- Penalty multiplier factor (f_P).
- Friction.
- Stabilization/stiffness multiplier factor (f_{stb}) (new sub-node in Structural Mechanics Module version 6.2).
- Union/Assembly flange/DVS.
- Gasket plasticity.

An extensive meshing investigation was performed for the DVS.

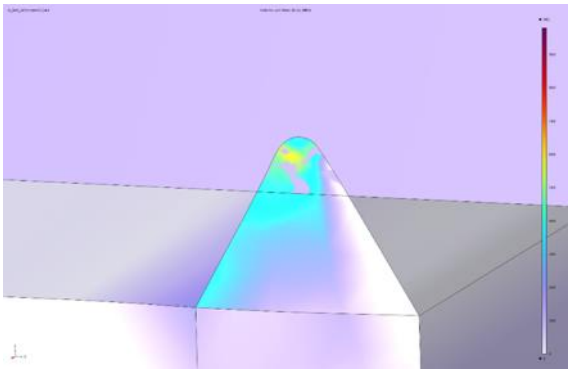

FIG. 21. Mesh penetration during 3D simulations

By modifying the DVS build and dividing the geometry into smaller domains it was possible to achieve better meshing at the ridge tops and the solution converged with an undamaged mesh, ref. Figure 21, however, still with some penetration.

For the mechanical models, both 2D-axisymmetric modelling and 3D modelling have been applied, applying the Solid Mechanics physics interface coupled with application of non-linear material modelling of the DVS.

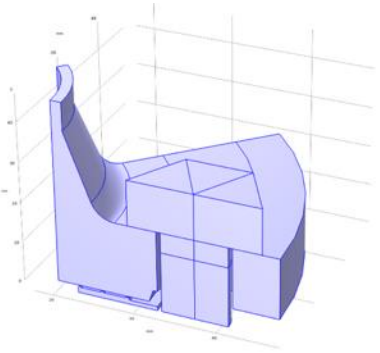

FIG. 22. 3D model of 1/8 part of bolted flange joint gasketed with DVS with M16 hex bolt

The 3D mechanical models simulate the conditions of a BFJ gasketed with DVS whereas the platens testing cases were modelled by 2D axisymmetric components. The 3D models (Figure 22) take advantage of several symmetries thereby reducing the model sizes and computation time for solving the models by limiting the size of the model to 1/8 of the full 4-bolt DN40 PN40 standard flange.

The COMSOL Part Library was investigated for the round bolt head modelling. However, it was decided not to apply the available models due to the lack of radius between the shank and the bolt head. This is not in accordance with international bolting standards (ASME) and large stress concentrations were also observed at this location during the early stages of the model development. Hence, the bolt was modelled from scratch and a radius of the fillet of 0.51 mm was introduced, see Figure 27 below.

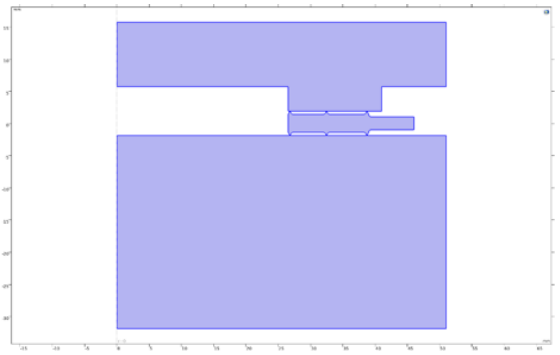

FIG. 23. 2D axisymmetric model of test set-up for EN 13555 testing of DeltaV-Seal

Figure 23 shows the principal parts the 2D axisymmetric model simulating the standard EN 13555 gasket testing equipment whereby the test sample (DVS), is placed on the lower (fixed) platen of the hydraulic press and the upper (movable) platen compresses the sample at the required/specified compression force (no internal pressure during these tests).

The two platens were equipped with transducers to measure the actual gasket thickness during the load ramping process and the test rig is required to have a defined total stiffness of 500 kN/mm when simulating EN-flanges and 1500 kN/mm when simulating ASME flanges.

This model also served as an initial “work horse” to develop a better understanding of the potential issues with non-linear small material volume FEA modelling of the 60 degrees DVS triangles to be used for the subsequent 3D modelling.

For the 2D axisymmetric models the segregated solver has been applied whereas for the 3D models the fully coupled solver has been applied with the non-linear iteration method changed from the standard double dogleg method to the constant Newton method with an increase of the maximum number of iterations from 25 to 50 to improve convergence.

3.4.2. Corrosion model

For the corrosion model 2D axisymmetric modelling has been applied.

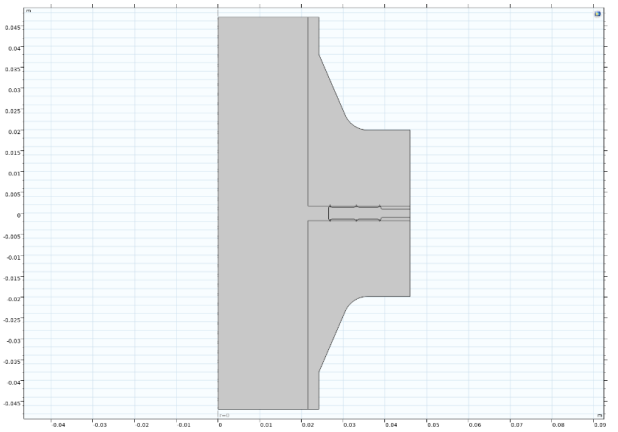

FIG. 24. 2D axisymmetric model of flange + DVS with electrolyte domains

The secondary current distribution physics interface was selected coupled with the Level Set (LS) physics interface which was applied to track the moving interfaces between the electrode domains (DVS ridges and the flange) and the electrolyte domain as the corrosion progresses by solving a transport equation for the level set function.

The LS physics interface was selected due to the challenging geometrical features at the DVS ridge top/flange surface interface as described above. Early attempts to apply

the Deformed Geometry/Moving Mesh interfaces were not successful. Furthermore, the highly conducted porous electrode interfaces were introduced for both the DVS and the flange (no bolts were included in the corrosion model).

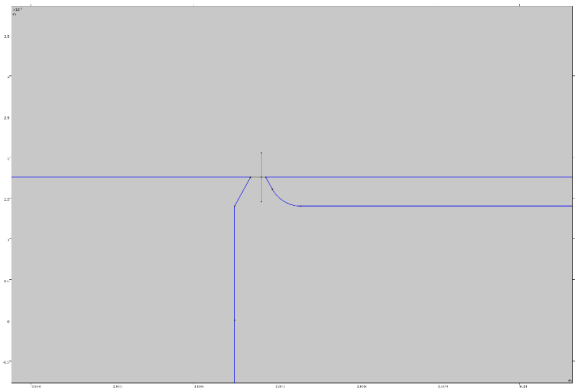

FIG. 25. Part of 2D axisymmetric model with the Level Set function located for break-through of ridge barrier (vertical line in grey).

The principals of the Level Set modelling approach are indicated in Figure 25 with the level set to an arbitrary penetration distance of 70% of the compressed ridge width considered to constitute a corrosion/material loss failure of the barrier, refer to the position of the line in 'grey'. At time zero the electrolyte model domain was set at an electrolyte/electrode ratio equal to one whereas the flange + DVS model domains were set an electrolyte/electrode ratio equal to almost zero (1e-6).

For the porous electrode reaction kinetics, a number of current density – electrochemical potential functions were developed based on the polarization curves that were obtained during the QEERI investigations as described above, see sections below. Such curves have been developed for several different materials and conditions relevant for the application of DVS in the energy industry. In the future, more such investigations are required both for validation of the models and for more realistic environments than the current 0.5 M NaCl solution.

For the electrolyte domain definition, the DVS/flange configuration was divided into several separate electrolyte domains which were activated individually as the galvanic corrosion process proceeds and eventually leading to breakdown of the ridge barriers or the flange surface depending on the conditions resulting in a corrosion/leakage failure.

Three study steps have been included in the corrosion model, namely:

1. Phase initialization
2. Current distribution initialization
3. Time dependent

3.4.3. Meshing

Several meshing investigations were conducted for the mechanical models.

The final 3D mesh was decided as three separate meshes, one for the bolt, one for the flange and one for the DVS. Due to the shape of the DVS triangles a separate swept meshing procedure was introduced for this component.

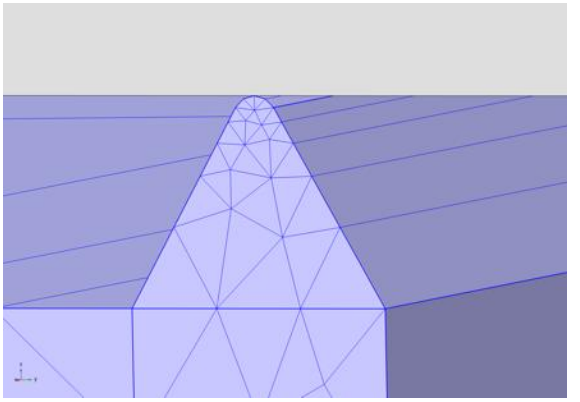

FIG. 26. Inner DVS ridge top triangle modelled with a 0.05 mm radius of the fillet and free triangular elements swept with extremely fine element size.

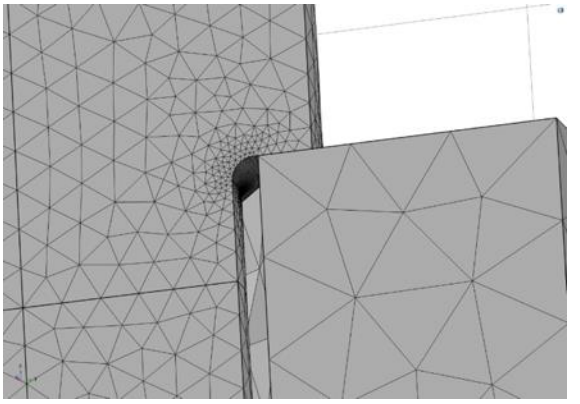

FIG. 27. Bolt meshed with extremely fine free tetrahedral elements and flange meshed with finer free tetrahedral elements with physics-controlled element sizes at the introduced shank/bolt head interface fillet with a radius of 0.51 mm.

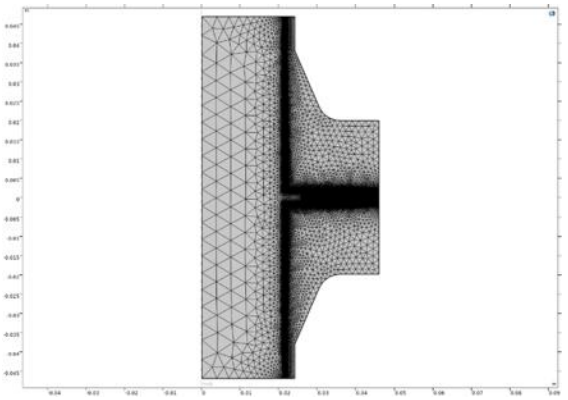

FIG. 28. For the porous electrode corrosion model, several sub-sets of the mesh were required to obtain a realistic/physical simulation of the solid flange/DVS components as highly conductive porous electrodes and discretization of the different electrolyte domains.

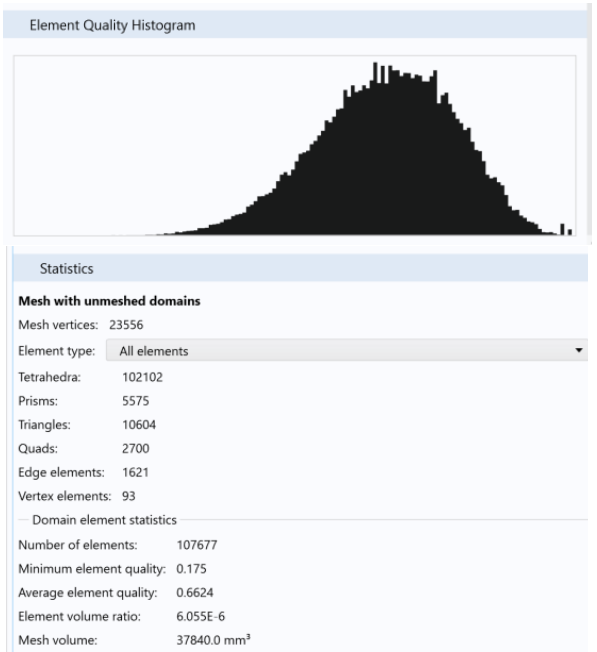

FIG. 29. Upper plot: the 3D mesh statistics showed an average element quality of 0.66 for the 107677 domain elements with a minimum quality of 0.175. Lower figure: A summary of the mesh quality statistics for the 3D BFJ model is shown in the table above. These statistics were deemed acceptable for the simulations.

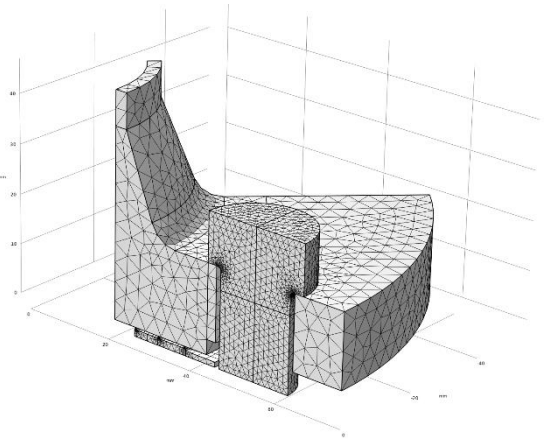

FIG. 30. Meshing of 1/8 part of 3D model of bolted flange joint gasketed with DVS and round M16X2 bolt.

4. Theory

4.1. Equations – Solid mechanics (3D model)

In accordance with (17), applicable PDE equation for the solid mechanics physics interface for Step 1 Bolt Pretension applied in the 3D model is as follows:

$$0 = \nabla \cdot (F S)^T + \mathbf{F}_V, \quad F = I + \nabla \mathbf{u2} \tag{1}$$

where

- **u2** is the dependent variable (displacement field)

- I is the identity matrix

- F is the deformation gradient tensor

- S is the second PK stress tensor

- $\mathbf{F}_V$ are the volume forces in the system, e.g., body loads, rotating frames, etc.

The PDE is the equation of motion with the acceleration set to zero. The bolt pretension study step is a special case of a stationary study step, where the special degrees of freedoms used for modelling prestressed bolts are solved for.

Three different stress measures are used in COMSOL Multiphysics:

- Cauchy stress σ defined as force/deformed area in fixed spatial directions not following the body. This is a symmetric tensor.
- First PK stress ***P***. The forces in the spatial directions are related to the area in the original (material) frame. This is an unsymmetric two-point tensor.
- Second PK stress ***S***. Both force and area are represented in the material configuration. For small strains the values are the same as Cauchy stress tensor, but the directions are rotating with the body. This is a

symmetric tensor. In geometrically nonlinear analysis, the stress should in general be interpreted as second PK stress, refer to the DVS stresses.

The PK stresses relate to each other as:

$$\boldsymbol{FS} = \boldsymbol{P} \tag{2}$$

In a geometrically linear analysis, the distinction between the stress measures disappears, and they all converge to the same values. This is the case considered for the bolt/flange (3D), and the platens (2D axisymmetric) in this Thesis.

4.1.1. Equations – Linear Elastic Material

In accordance with the theory of elasticity, for the linear elastic material model, Hooke's law relates the stress tensor to the elastic strain tensor:

$$\sigma = \sigma_{ex} + \mathbb{C} : \varepsilon_{el} = \sigma_{ex} + \mathbb{C} : (\varepsilon - \varepsilon_{inel}) \tag{3}$$

where $\mathbb{C}$ is the 4th order elasticity tensor, ":" stands for the double-dot tensor product (or double contraction). The elastic strain ε_{el} is the difference between the total strain ε and all inelastic strains ε_{inel}. There may also be an extra stress contribution σ_{ex} with contributions from initial stresses and viscoelastic stresses. In case of geometric nonlinearity, the second PK stress tensor and the Green-Lagrange strain tensor are used.

For the flange and the bolt in the 3D model as well as the solid platens in the 2D axisymmetric model, an isotropic material and elastic moduli have been considered for which the $\mathbb{C}$ tensor reduces to:

$$D = \frac{E}{(1+\nu)(1-2\nu)} \begin{bmatrix} 1-\nu & \nu & \nu & 0 & 0 & 0 \\ \nu & 1-\nu & \nu & 0 & 0 & 0 \\ \nu & \nu & 1-\nu & 0 & 0 & 0 \\ 0 & 0 & 0 & \frac{1-2\nu}{2} & 0 & 0 \\ 0 & 0 & 0 & 0 & \frac{1-2\nu}{2} & 0 \\ 0 & 0 & 0 & 0 & 0 & \frac{1-2\nu}{2} \end{bmatrix}$$

Hence, the only required input values are the Poisson's ratio and the Young's modulus. Tabulated values for the flange and the bolt (alloy 800HT) and structural steel (platens) have been considered.

4.2. Equations – Secondary current distribution (2D axisymmetric)

The applicable PDE equations for the secondary current distribution physics interface are as follows:

$$\nabla \cdot \mathbf{i}_l = Q_l, \quad \mathbf{i}_l = -\sigma_l \nabla \phi_l \tag{4}$$

$$\nabla \cdot \mathbf{i}_s = Q_s, \quad \mathbf{i}_s = -\sigma_s \nabla \phi_s \tag{5}$$

$$\phi_l = \text{phil}, \quad \phi_s = \text{phis} \tag{6}$$

The applicable PDE equations for the level set physics interface are as follows:

$$\nabla GI \cdot \nabla GI + \sigma_w GI \nabla \cdot \nabla GI = (1 + 2\sigma_w) GI_i = -k \nabla \emptyset \tag{7}$$

$$\frac{\partial \phi}{\partial t} + \mathbf{u} \cdot \nabla \phi = \gamma \nabla \cdot \left(\varepsilon_{ls} \nabla \phi - \phi(1-\phi) \frac{\nabla \phi}{|\nabla \phi|} \right) \tag{8}$$

4.2.1. Electrochemical corrosion

In accordance with (16), the current density in a dilute electrolyte system can be expressed as

$$i = -F \sum_i z_i D_i \nabla c_i - F^2 \nabla \emptyset \sum_i z_i^2 u_i c_i + F v \sum_i z_i c_i \tag{9}$$

Where

- 1st term is diffusion.
- 2nd term is migration.
- 3rd term is convection.

And

- c_i is the concentration of species i
- D_i is the diffusivity of species i
- z_i is the charge number of species i
- F is Faraday's constant
- $\emptyset$ is the electrical potential
- u_i is the electrochemical potential of species i
- v is the fluid velocity

In this Thesis work, it is assumed electroneutrality in the corrosion system and hence

$\sum_i z_i c_i = 0$ (the 3rd term vanishes).

Furthermore, it is assumed that the contribution from diffusion as a result of concentration gradients is much smaller than the effect of migration and therefore equation (7) reduces to the common concept of electrolyte conductance, namely

$$i = -k \nabla \emptyset \tag{10}$$

Where the conductivity

$$k = F^2 \sum_i z_i^2 u_i c_i i = -k\nabla\emptyset \quad (11)$$

And by applying charge conservation ($\nabla i = 0$) the Laplace can be obtained which is the governing equation for the secondary current distribution adopted for the corrosion model:

$$\nabla^2\emptyset = 0 \quad (12)$$

As mentioned in this Thesis, the galvanic corrosion model is assumed to be conservative since the full Nernst-Planck mass transport physics interface (tertiary current distribution) has not been adopted and only charge transfer has been assumed. The use of the Laplace approach relies instead on the availability of laboratory test data (e.g. polarisation curves) for the electrodes and knowledge about the electrolyte characteristics (primarily the conductivity).

4.3. The Level set method

The level set (LS) method in COMSOL is a technique to represent moving interfaces or boundaries using a fixed mesh, it is available in the Corrosion module. It is useful for problems where the computational domain can be divided into two domains separated by an interface which is the case in the DVS/flange configuration.

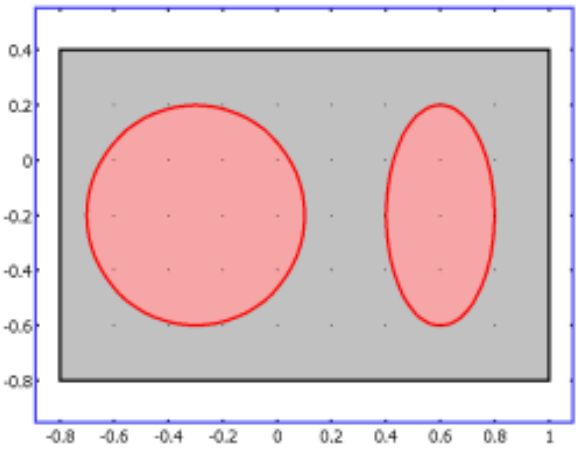

FIG. 31. The Level Set method principle (from Comsol Help).

Each of the two domains can consist of several parts, refer to the figure to the left which shows an example where one of the domains consists of two separated parts. The interface is represented by a certain level set or iso-contour of a globally defined function, the level set function ϕ.

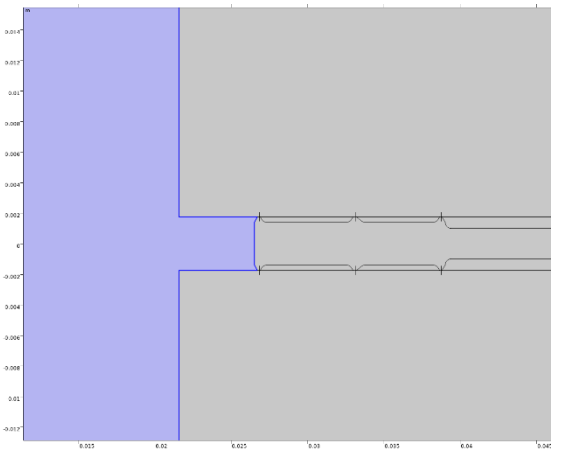

FIG. 32. Electrolyte domain and "empty" electrolyte domains connected via the LS function which is activated after the 1st barrier breakdown.

In COMSOL Multiphysics, ϕ is a smooth step function that equals zero (0) in one domain and one (1) in the other. Across the interface, there is a smooth transition from zero to one. The interface is defined by the 0.5 iso-contour, or level set, of ϕ. The figure below shows the level set representation of the interface in the figure above.

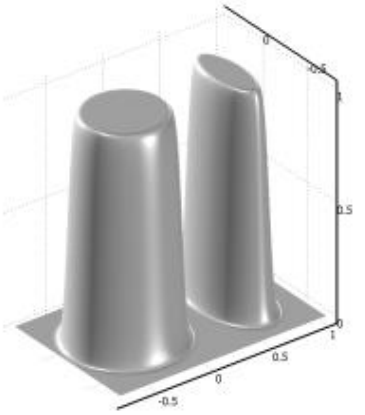

FIG. 33. Surface plot of the Level Set function corresponding to Figure 30 (from Comsol Help).

The physics interface solves equation (7) to move the interface with the velocity field **u.**

The terms on the left-hand side give the correct motion of the interface, while those on the right-hand side are necessary for numerical stability. The parameter, ε_{ls}, determines the thickness of the region where ϕ varies smoothly from zero to one and is typically of the same order as the size of the elements of the mesh.

By default, ε_{ls} is constant within each domain and proportional to the largest value of the mesh size, *h*, within the domain. The parameter γ determines the amount of reinitialization or stabilization of the level set function. It needs to be tuned for each specific problem. If γ is too small, the thickness of the interface might not remain constant and

oscillations in ϕ can appear because of numerical instabilities. On the other hand, if γ is too large the interface moves incorrectly. A suitable value for γ is the maximum magnitude of the velocity field **u**.

All these parameters were tweaked in the corrosion model to achieve a realistic corrosion/weight loss front progression from the flange inside to the outside with a reasonable convergence/computation time. The current model is set at an arbitrary point of barrier break-through at 70% of the ridge top flattened radial distance counting from inside.

5. Results and discussion

5.1. 2D axisymmetric modelling (mechanical)

The purpose of this modelling was to simulate the mechanical testing in accordance with (11). The DVS thickness reduction resulting from the compression (ref. to Section 2.4) is the DVS response to the applied compression force and is a fundamental property of all gaskets required for the design of BFJ in accordance with the pressure vessel codes ((13), (15)).

The simulation was performed by adding a defined target compression as a prescribed displacement boundary condition and applying an auxiliary sweep from zero to approximately 0.5 mm displacement corresponding to a relatively high bolt-up compression for DVS and plotting the model output in the form of reaction force for comparison with the experimental applied force – thickness reduction function.

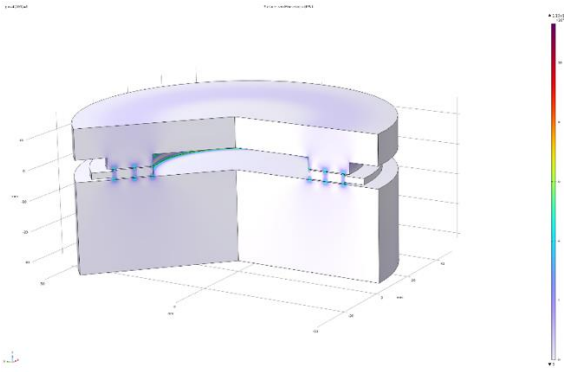

FIG. 34. 3D plot of von Mises stresses at maximum compression for an early-stage model of the platens configuration (later modified).

An application was developed on this model to streamline investigation and result presentation of systematic variation of the target compression and the resulting total reaction forces. The purpose of this investigation was to benchmark the model and the simulation results against the measured reaction forces during the EN 13555 laboratory testing.

The results show that the simulated total reaction force for the maximum set gasket compression (0.25 mm x 2 = 0.50 mm) of 100 kN (see plot below) whereas the testing showed a compression force of nearly 240 kN, refer to purple curve in Figure 35. More simulations are required to explain this difference which will be performed during the subsequent phases of the project.

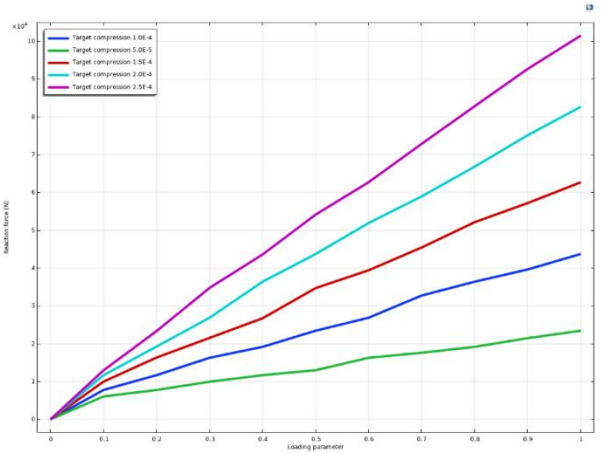

FIG. 35. Application plot of the resulting ramping load vs. reaction force for five different target compression levels.

However, the geometrical performance of this model is satisfactory in regards of the simulated plastic deformation of the ridges, hereunder the flattening, see plot below.

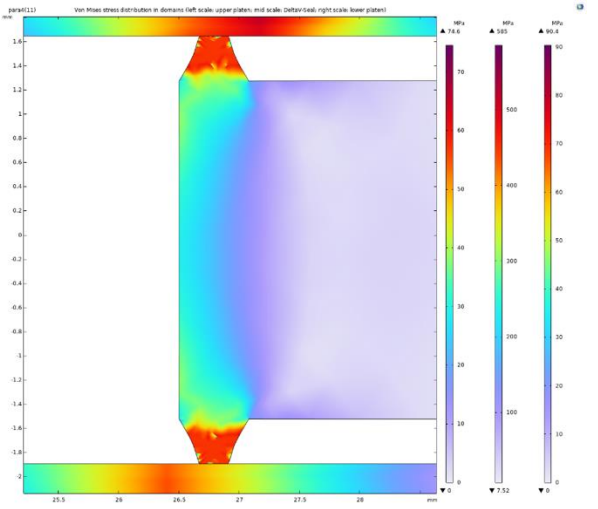

FIG. 36. Stress distribution plot showing the flattening behaviour at large equivalent plastic strains.

In the next phases of the project optimization algorithms will be developed to simulate the effect of varying the number, distribution, and geometry of the ridges across the DVS core to achieve the lowest possible reaction force for a minimum level of compression for the bolt-up stage of the BFJ, see below.

5.2. 3D modelling (mechanical)

Several boundary, edge and point probes were defined for monitoring important aspects of the 3D simulations and bench marking and model validation against the results of the laboratory investigations:

- Type A: The width of the ridges (ref. metallurgical investigations)
- Type B: The area of the ridge triangle base areas (ref. gasket stress calculations)
- Type C: The rotation of the flange (ref. BFJ design code requirements)

Standard industry LC's were defined and simulated, namely:

- LC 1: Assembly and bolt-up (bolt pretension)
- LC 2: Pressure testing
- LC 3: In-service conditions (external force and moment loads from adjoining piping)

For all LC simulations, different loading ramping factors were tested in parametric sweeps to facilitate convergence and control and monitoring of the solver log during the computations.

Simulation of LC 1 required solving for 492436 DOF's plus 811137 internal DOF's with a computation time of 34 minutes applying the modified fully coupled solver.

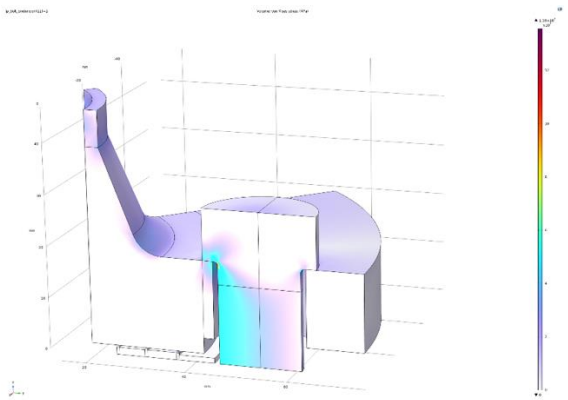

FIG. 37. von Mises stress distribution in the BFJ, due to the pivoting effect of the DVS, the stress distribution in the bolt shows the highest stresses closet to the DVS.

The presented LC 1 involves a bolt pretension load of 62545 N which is the highest pretension load normally applied for this BFJ gasketed with DVS. Since this BFJ design includes 4 bolts, the total pretension force is 4 x 62545 = 250180 N during assembly of the BFJ, ref. also to Figure 12.

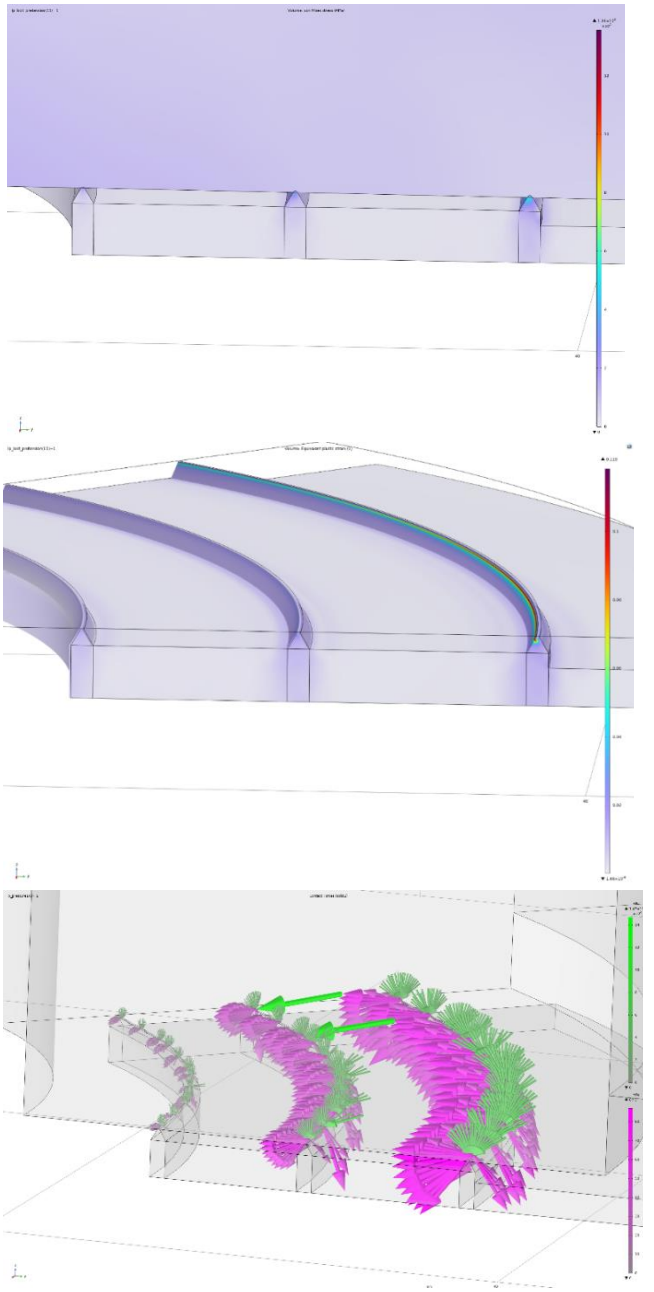

FIG. 38. a) The upper plot shows that the outer ridge closest to the bolt has the highest stresses underpinning the location of the pivoting effect of the outer ridge. This is also in line with the results presented in (5) for flat rectangular cross sections of non-metallic gaskets. b) The middle plot shows that the maximum equivalent plastic strain is almost 12% at the outer ridge. c) The lower plot shows the complex and non-uniform contact pressure distribution at the ridges after bolt pretension and an added 40 bar internal pressure.

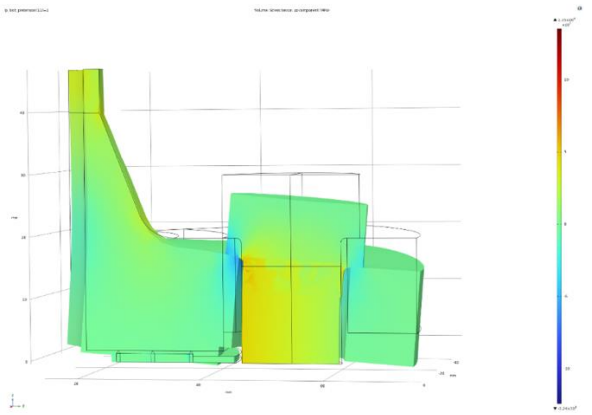

FIG. 39. Stress distribution in the bolt during LC 1 and scaled-up view of the flange rotation.

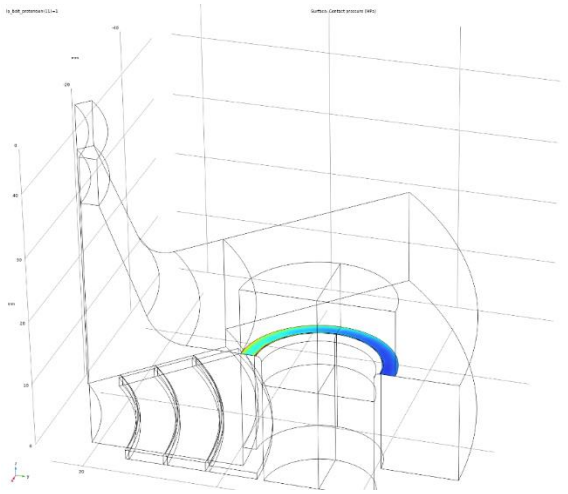

FIG. 40. Contact pressure distribution at the bolt head/flange surface interface with the highest contact pressure closest to the DVS.

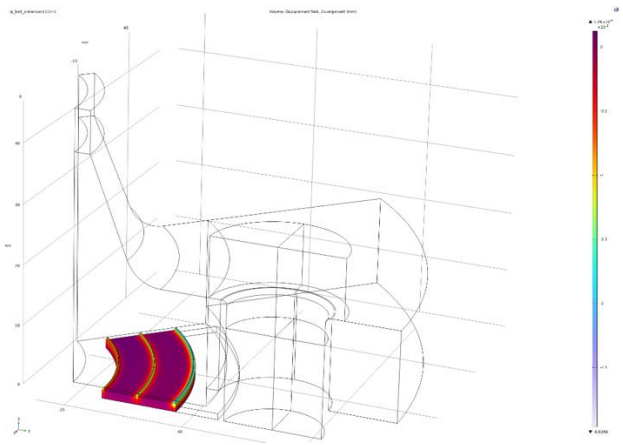

FIG. 41. Z-component displacement field distribution for the DVS indicating that the core of the DVS is not subjected to any loads but is acting as a support for the sealing ridges with the largest displacement occurring on the outer ridge closest to the bolt.

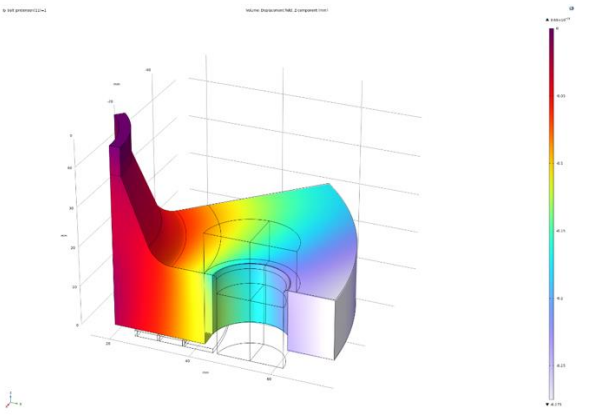

FIG. 42. Flange rotation distribution with a maximum at the outer edge of the flange of 0.275 mm.

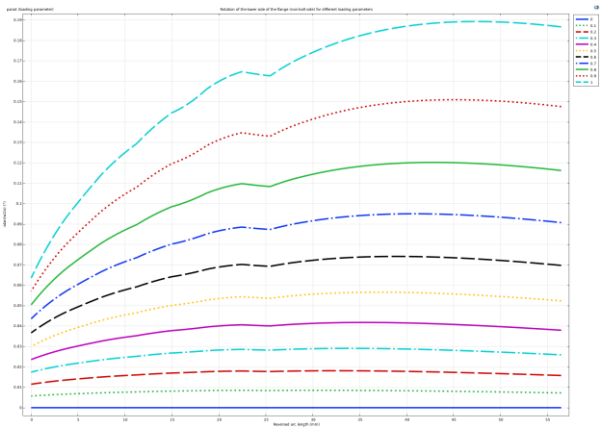

FIG. 43. Summary of flange rotation development during load ramping steps along the lower side of the flange.

The displacement distribution shown in Figure 42 has been transformed to flange rotation given in degrees. The above plot (Figure 43) shows the flange rotation as a function of the position from the bore of the flange to the outer edge using the probe data located at the lower edge boundary of the flange on the non-bolt side of the flange – one curve for each load ramp.

The results show a maximum rotation of approximately 0.19 degrees well below the ASME/EN design code requirements for BFJ.

During the 3D simulations some penetrations have been noted (refer to Figure 44) despite the extensive efforts to eliminate/reduce this behavior as stated above. However, it was deemed acceptable for the current assessments due to the overall as expected general behavior of the simulations. However, this will be further elaborated on in the next phases of the project in addition to further fine tuning of the model parameters to clearly define acceptable parameter windows for LC 3 (lateral, axial, and bending loads).

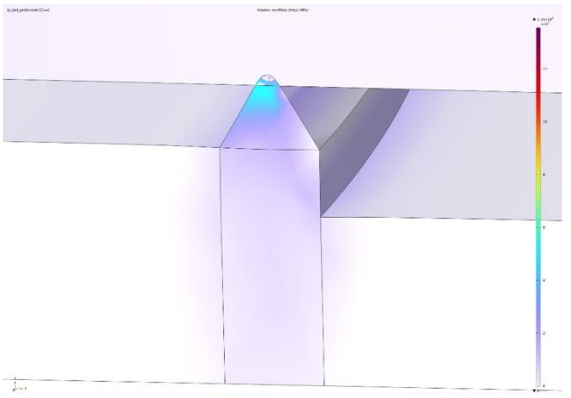

FIG. 44. 3D simulation – typical mesh penetration.

5.3. 2D axisymmetric modelling (galvanic corrosion)

For the galvanic corrosion simulations, several different polarization functions have been developed for the secondary current distribution physics interfaces. These functions had to be based on developing a smoothing function to be applied on the polarization data received from the testing laboratory (Excel data, ref. to Section 2.2), otherwise the models did not converge with reasonable computation times.

The following flange/DVS materials in different combinations have been simulated for galvanic corrosion at the flange/DVS contact points and time for breakthrough of the sealing ridges:

1. 316L_DVS-undef_QEERI_0.5M_NaCl_sample_A4.1
2. B4 316L
3. F2-F3
4. UNS S30400 (stainless steel) in 5 M HNO3
5. A105 flange
6. S235-E3 sample (no zinc)

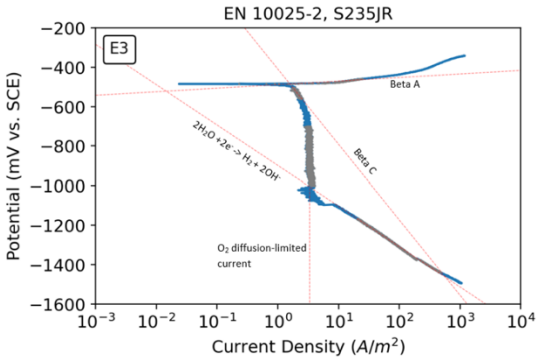

FIG. 45. Polarization curve obtained for the gasket material (sample E3) with a corrosion potential of -486 mV SCE.

The polarization curve shown in Figure 45 was subjected to smoothening and applied as the local current density interpolation function for the DVS electrode in the galvanic corrosion model.

For the flange electrode the polarization curves shown in Figure 46 below were averaged and subjected to the smoothening function and applied in the galvanic corrosion model as the local current density interpolation function for the flange electrode. Note that the average corrosion potential for the flange material is -520 mV SCE.

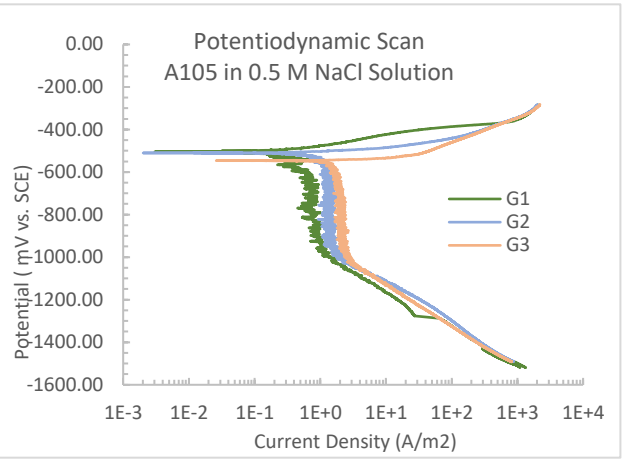

FIG. 46. Polarization curves obtained for the flange material with an average corrosion potential of -520 mV SCE.

During these simulations, both the flange and DVS were modelled with the highly conductive porous electrode domain features with a tortuosity conductivity correction.

For the presented case and based on the laboratory polarization curves, the local current density expressions were limited to 3 and 1.3 A/m^2 for the DVS and flange respectively which are normal values for 0.5 M NaCl solutions, refer to the polarization curves above. As mentioned before, the current model predictions are conservative due to the not-included formation of protective corrosion products and in the case of stainless steels the formation of protective passive films and hence the considered kinetic reactions are only the charge-transfer (active corrosion) part of the polarization curves, ref. plots above.

This case simulates the galvanic corrosion effect between a flange in a standard carbon steel material (A105) and a DVS in the standard carbon steel material S235.

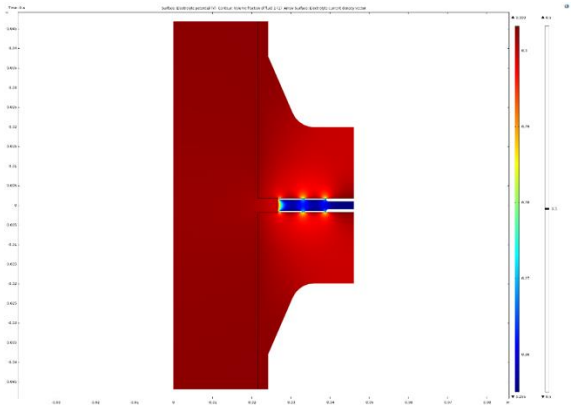

FIG. 47. Simulated electrolyte potential distribution at time zero indicating that the DVS will be nobler than the flange in this galvanic couple. The plots show a potential difference of 48 mV to be compared with the measured corrosion potential difference of 34 mV.

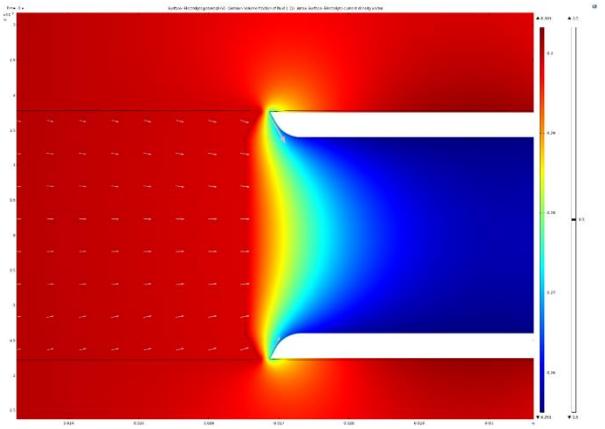

FIG. 48. Direction of the electrolyte current density vectors from the flange to the DVS underpins that the flange material would be anodic to the DVS in this galvanic cell thereby causing an increased local corrosion damage of the flange surfaces at the interface with the DVS ridges.

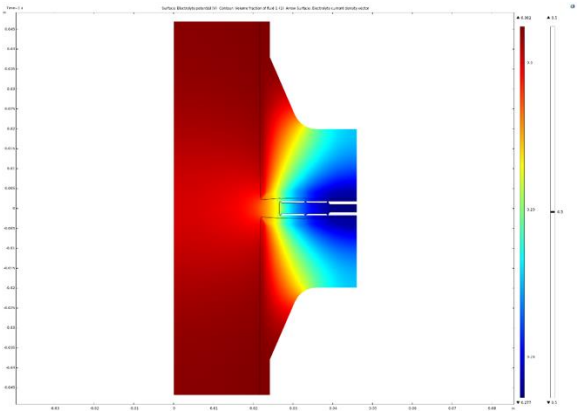

FIG. 49. Plot show a 1-year simulation of the electrolyte potential distribution where the electrolyte potential drop goes from the flange to the DVS as discussed above with a material loss indicated in the flange surfaces which would (in theory) cause a leakage of the BFJ. In the model the local current densities have been transformed to material loss via Faraday's law.

It should be noted that a potential difference between the electrodes in the range of 25 to 50 mV should be acceptable, ref. to discussion above, but the current model is conservative since the formation of protective corrosion products is not included.

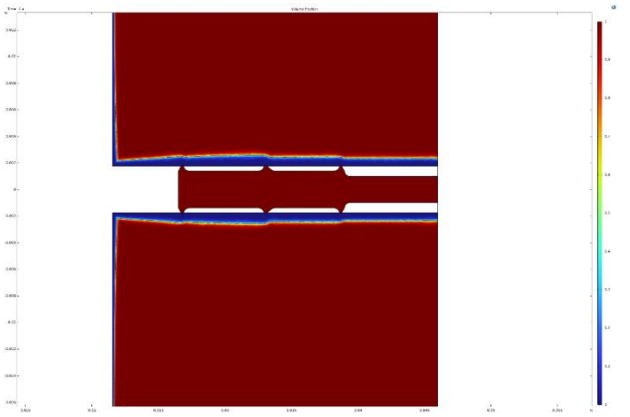

FIG. 50. Electrolyte ratio of the porous flange and DVS domains after a 1-year simulation indicating the anodic behavior and material loss of the flange due to galvanic corrosion (blue regions indicating electrode/electrolyte ratio equal to zero). This configuration would then constitute a complete corrosion failure of the BFJ and associated leakage.

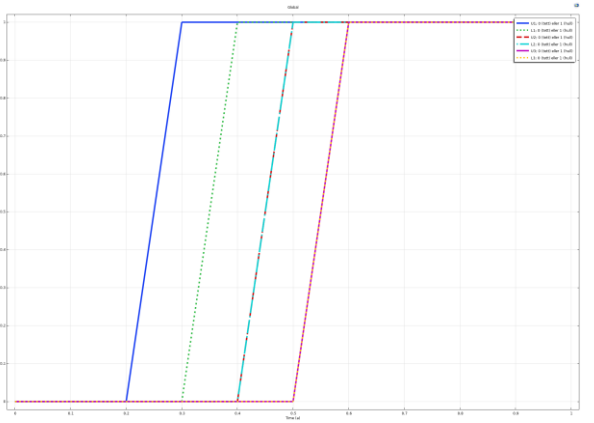

FIG. 51. Summary of 1-year simulation; electrolyte volume fraction related variables called U1/U2/U3/L1/L2/L3 as a function of simulation time

For illustration of the usefulness of this model, namely prediction of time to leakage, Figure 51 shows the 1-year simulation by plotting some electrolyte volume fraction related variables called U1/U2/U3/L1/L2/L3 as a function of simulation time. Note that the variables U1/U2/U3/L1/L2/L3 correspond to the six electrolyte domains and a variable value = 0 corresponds to 'tight' and a parameter value = 1 corresponds to 'open/hole', refer also to the LS method description in Section 4.3.

The plot indicates that the 1st barrier would be corroded through after (0.2-0.3)*12 year, the 2nd barrier corroded

through after 0.4*12 year and final breakthrough of the 3rd barrier after 0.5*12 years at which point there would be leakage of the BFJ.

5.4. Future modelling

During the next phases of the project, the mathematical theory for fluid flow leakage calculations (7) will be codified in COMSOL and implemented in the sub-models as mentioned in this Thesis. Furthermore, it is intended to add a tertiary current distribution feature to the corrosion model to reduce the conservatism of the simulation by the formation of corrosion products well known to reduce the corrosion rates of carbon steels by resistance polarization. It will also be required to develop an interface model for the interaction between large plastic deformation and corrosion behavior.

The completed sub-models will then be integrated into a single knowledge platform for simulation of time to leakage of BFJ gasketed with DVS under assembly, testing and service conditions thereby predicting the required level of ridge compression during assembly to obtain the optimum leakage performance during service.

In the final phase of the project, several laboratory testing programs will be executed for validation and calibration of the models. These testing programs will have to be designed efficiently based on e.g. the Box-Behnken optimization theory due to the large number of factors/parameters impacting on the leakage performance of BFJ's as described in this Thesis including temperature and material selection.

Based on the completed and validated knowledge platform, several Applications will be developed and distributed to PoT's internal and external stakeholders underpinning PoT's business development strategy. These applications may then also be utilized for optimization of the number, distribution, and geometry of the sealing ridges across the DVS core depending on each specific customer requirement.

6. CONCLUSIONS

The fully metallic DVS gasket has been modelled for finite element analysis applying the COMSOL Multiphysics software. Both 2D axisymmetric and 3D space dimensions have been considered when simulating standard laboratory gasket compression testing as well as during assembly of bolted flange joints containing DVS.

The modelling and simulation work performed during the MT have been focused on achieving models that – as far as possible – simulates the available laboratory and other types of testing results. After model improvements, they can then be built on for optimization and application building in the next phases of the project.

Some main conclusions can be drawn from the work as follows:

- The distribution of the contact conditions is observed to be non-uniform across the gasket width with higher contact stresses and strains at the outer ridge compared to the inner ridge.
- The studied DVS configuration (number, positions, and geometry of the sealing ridges) is not optimized in the current product version. This will be further explored in subsequent phases of the project.
- The Level Set (LS) method gives a reasonable representation of the corrosion front progression throughout the flange joint, but the LS model parameter settings is a challenging task and needs further optimization for other materials and environmental conditions.
- The mechanical models are considered to behave reasonably well in replicating laboratory testing results but need further improvements in the next phases of the project, especially on the 3D model mesh penetration into the flange domain which must be mirrored correctly against practical experience of DVS installations in BFJ as well as the ridge flattening predictions.
- The galvanic corrosion model simulates well the expected corrosion potential difference between the flange and the DVS at the point of contact at initialization.

7. ACKNOWLEDGEMENTS

The authors gratefully acknowledge the technical and academic support of the following parties:

- Multiphysics Modeling School (https://www.multiphysics.uma.es)
- COMSOL Support, Trondheim, Norway
- COMSOL Support, Stockholm, Sweden

This study has been partly funded by the Research Council of Norway (SkatteFUNN).

8. ABBREVIATIONs

The following symbols and shortages are used throughout the report:

- DVS - DeltaV-Seal
- BFJ - Bolted flange joint
- PoT - Pipeotech AS
- QEERI - Corrosion Center of Qatar Environment & Energy Research Institute
- SCE - Saturated calomel electrode
- 800HT - UNS N08811 Fe-Cr-Ni alloy

- PDE - Partial differential equation
- PK - Piola-Kirchoff
- WN - Weld neck
- RF - Raised face
- LC - Load case
- DOF - Degree of freedom

9. REFERENCES

1. Necking of an Elastoplastic Metal Bar; COMSOL Multiphysics Application Library
2. Engineering work of Sanicro 31HT/800HT at ambient and elevated temperature; Report No. 12/2021, Przemyslaw Jaszak, Krzysztof Podkomorzy, Wroclaw University of Science and Technology, Faculty of Mechanical and Power Engineering, Wroclaw Poland, June 2021
3. Hardness measurements and examinations of undeformed and deformed gaskets in 316L, DNV GL AS Oil & Gas, Report No. 2020-3268, Rev. 00, Document No. 1031369, 16.12.2020
4. Determination of true stress-strain curve of type 304 and 316 stainless steels using a typical tensile test and finite element analysis; Hyeong Do Kweon, Jin Weon Kim, Ohseop Song, Dongho Oh, Korea Hydro & Nuclear Power Co., Ltd. 70, 1312-beongil, Yuseong-daero, Yuseong-gu, Daejeon, 34101, Republic of Korea
5. A study of the sealing performance of bolted flange joints with gaskets using finite element analysis; M. Murali Krishna, M.S. Shunmugam, N. Siva Prasad, Department of Mechanical Engineering, Indian Institute of Technology Madras, Chennai 600036, India
6. Prestressed Bolts in a Tube Connection; COMSOL Multiphysics Application Library
7. Leakage modelling through metal-to-metal contact surface and its implementation to predict tightness level of flange bolted joints sealed with DeltaV-Seal; Przemyslaw Jaszak, Wroclaw University of Science and Technology, Faculty of Mechanical and Power Engineering, Wroclaw Poland, 2023
8. Pipeotech – Seal Analysis; EDR Medeso, 07.01.2021
9. Pipeotech – Seal Analysis; EDR Medeso, 06.07.2020
10. Pipeotech – Seal Analysis; EDR Medeso, 26.08.2020
11. EN 13555:2021; Flanges and their joints - Gasket parameters and test procedures relevant to the design rules for gasketed circular flange connections
12. EN 1591-1:2013; Flanges and their joints - Design rules for gasketed circular flange connections - Part 1: Calculation
13. ASME Boiler and Pressure Vessel Code: 2023; Section VIII Rules for Construction of Pressure Vessels, Division 1, Mandatory Appendix 2
14. EN 1092-1: 2018; Flanges and their joints, Circular flanges for pipes, valves, fittings and accessories, PN designated, Part 1: Steel flanges
15. EN 13445-3:2021 Unfired pressure vessels - Part 3: Design
16. Mathematical Modeling of Potential and Current Distribution for Atmospheric Corrosion of Galvanic Coupling in Airframe Components; NACE Corrosion 2015 Paper No. 5579, C. Liu, V.N. Rafla, J.R. Scully, R.G. Kelly, Center for Electrochemical Science and Engineering, University of Virginia, Charlottesville, VA 22904